Quantitative and Computer-Aided Thermography-Based Diagnostics for PV Devices: Part I - Framework

A Quantitative and Computer Aided Thermography-based Diagnostics for PV Devices: Part I – Framework

S. Vergura, *Senior Member, IEEE*, and F. Marino

Abstract — **Although recent laboratory tests are showing promising progresses in the materials and production technologies of photovoltaic devices, the commercial PV modules do not show analogous impressive improvements. Therefore, a diagnostic approach, able to check the current state of health of already installed PV systems, as well as their trend of ageing, assumes a strategic importance. In this scenario, we introduce a thermography-based diagnostics able to provide a detailed, clear and unambiguous information, thanks to a computer aided investigation that is much deeper than the today available infrared analysis. The proposed approach allows a numerical and qualitative evaluation of each cell of the PV device.**

This *Part I – Framework* introduces the methodology, based on two main analyses. The first one (*cell analysis*) studies each single cell, while the second one (*cluster analysis*) focuses the attention on groups of PV cells. The framework is also characterized by a pre-processing in which the Region of Interest is extracted from the infrared image in order to focus the successive processing and analyses only on this area. The P*art II – Platform and Results* shows the cloud platform implementing the workflow (it automatically generates a comprehensive and detailed report), and discusses also several significant cases of study.

Index Terms — **thermography, computer aided diagnostics, digital image processing, PV cells, PV modules, PV devices, filtering.**

I. Introduction

According to a recent study of the Fraunhofer Institute for Solar Energy Systems (ISE), the maximum Photo Voltaic (PV) cell efficiency reached today is 46.0%, but this performance has been effectively obtained only in laboratory experiments [1]. The previous record of efficiency (44.7%) was obtained by the same ISE, and has been presented in literature [2]. These values (as well as other performances since 1976), have been summarized by the National Renewable Energy Laboratory (NREL) in a well-known diagram [3].

Anyway, less exultantly, the efficiency of commercial PV modules goes from 8% to 22% (the lower bound being referred to the amorphous and organic PV cells, the higher one to the mono-crystalline ones).

Sometimes the power losses are due either to the dust or to the dirt on the PV module, but they also may depend on internal problems of the cells. In these last cases, they manifest themselves as temperature increases, as reported in Table 3 of [4].

An abnormal over temperature of a PV cell (say, hot cell) causes a drastic efficiency loss, affecting the energy production: it results that a temperature increase of 10 °C for the cell surface provokes about 4% power loss (we say this hot cell *light*), while an increase of 18 °C reduces the power of about 7÷10% (we say this hot cell *strong*).

When internal problems arise, they are classified as *defects* and are essentially grouped in two main typologies [5]-[7]: *material-induced* (depending on the internal material structure), and *process-induced* (generated during the productive process). In order to deeper investigate these phenomena, some specific and known defects have been modelled and inserted in well-operating PV cells, and their thermal effects have been analyzed, mainly by means of the Finite Element Method (FEM) [8], [9].

In fact, FEM is largely employed to study effects in industrial applications for diagnostic purposes, thus, for instance, in [10], it has been also used to model three different typologies of defects which commonly appear in PV modules (linear edge shunt and hole for mono-Si and poly-Si cells, conductive intrusion for amorphous-Si cells), obtaining a punctual analysis of the over temperatures. Anyway, these typologies of defects are not the only ones already known (e.g., entrapped air, non-linear edge shunt, Schottky-type, scratches, aluminum particles, and so on), whereas many other defects are still neither defined nor modelled: anyhow, though this field is surely an important and open research area to be investigated in the future, it has been already clarified that *defects manifest themselves as over temperatures*. Since a PV module cannot be point-to-point investigated by means of a thermometer, the issue is overcome by means of thermography, which allows both to highlight hot spots and to perform an efficient and systematic investigation on typical defects in solar cells [11]. For instance, in [12] the thermographic analysis is used to identify the mismatch faults of PV modules; in [13] it is used for detecting snail trails and cell micro-cracks, and in [14] the thermography is proposed for improving the energy efficiency under partial shading conditions. Moreover, in [15], its employment for controlling the quality of PV modules is compared to other non-destructive techniques, such as electro- and photo-luminescence imaging and [16]-[17] propose combined techniques of both luminescence and thermography during the

S. Vergura is with the Department of Electrical and Information Engineering, Politecnico di Bari, Italy (e-mail: silvano.vergura@poliba.it). *Corresponding author*.

F. Marino is with the Department of Electrical and Information Engineering, Politecnico di Bari, Italy and with the Spin-off APIS-Apulia Intelligent Systems (e-mail: f.marino@spinoffapis.com).

production process. Now, though a comparison between luminescence imaging and lock-in thermography proves that there is no predominance of one technique over the other one in detecting defects in solar cells (as Table I of [18] demonstrates), of course thermography shows some advantages on the other techniques. In fact, today, it represents a consolidated tool for diagnostic purposes for several reasons, such as robustness and availability of:

- portable and fixed thermo-cameras;
- low-cost devices;
- several typologies of sensors (as it will be better explained in the successive section), and so on.

For example, an automated control system for PV plants, able to distinguish a defected module from a well working one has been recently proposed [19], which is based on an unmanned aerial vehicle, embedding an IR camera.

This scenario motivates this paper at proposing a diagnostic workflow for carrying out an accurate quantitative analysis of PV devices, up to the level of each single cell, based on the automatic processing of InfraRed (IR) images, that has been also implemented on a cloud platform [20], whose details are given in Part II [21]. The diagnostic approach has been developed and tested for different PV devices. Among them, those having larger diffusion and greater economical emphasis are the PV modules, which have been used as cases of study, widely discussed in [21].

This paper is structured as follows. Section II briefly describes the relations among the bands of the IR spectrum, the sensors of the thermo-cameras and the behavior of the glass superimposed on the PV module. Section III presents the diagnostic workflow and illustrates its main steps, while Conclusions ends the paper.

II. IR ANALYSIS AND THERMAL-CAMERA SPECIFICATIONS

Fig. 1 reports a wavelength diagram, zooming on the *visible* and *IR* spectrums: as it is shown, the IR band comes immediately after the *red* color of the visible spectrum, from which takes its name. Moreover, it is usually divided into other sub-bands, defined by the adjectives near- (from the superior limit of the visible range), shortwave-, midwave-, longwave-.

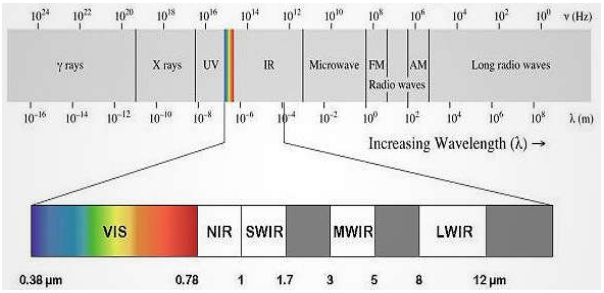

Fig. 1. Near-, shortwave-, midwave-, longwave- infrared sub-bands.

It is extremely important to properly take into account the IR spectrum composition, when one has to perform an IR acquisition of PV devices. This, at least for two reasons: 1) the thermal sensor of the camera captures the radiation within a specific spectral range, and not in the whole IR spectrum (therefore, it is very important to know the specifications of the employed thermal-camera); 2) the glass protecting the PV device, said solar glass, assumes a different behavior, with respect to the wavelength of the emitted radiation (opaque for the long-wave IR and transparent for the mid-wave IR).

With respect to the second point, there is a great difference if the IR acquisition is made by means of a midwave thermal-camera or through a longwave one. The thermal-cameras operating in the midwave IR range are very sophisticated from the technological point of view, because they need a cooling system for the thermal detector. This makes them very expensive and less diffuse. Instead, the thermal-cameras operating in the longwave IR range use a micro-bolometer as thermal detector. This sensor stresses the detector material heating it, and changing its electrical resistance: the resulting variation are transduced into temperatures, which are finally quantized in the pixels of the IR image. The micro-bolometer does not require cooling; consequently, the technology of the long-wave IR thermal-cameras results simpler, leading to a lower price and a larger diffusion. However, unfortunately, IR images acquired by means of a long-wave IR thermal-camera represent the temperature map of the glass on the PV device, and not the temperature map of the PV cells. This mismatch is caused by the opacity to the long-wave IR of the solar glass, and in our experience is usually contained in the range 1÷3 °C, mainly depending on the glass thickness and on the iron percentage. For these reasons, the awareness of the typology of the employed thermal-camera is needed in order to know if the temperature map (i.e., the IR image) has to be intended as referred to the PV cells or to the solar glass. After having remarked that the above mismatch becomes more relevant when the temperatures of the PV cells are different enough, causing an inaccurate diagnostics, we point out that the software platform [21], implementing the here proposed workflow, is compatible with both the mid-wave and the long-wave thermal-cameras. In fact, in the preliminary INPUT stage, the software asks the user to select the typology of the IR camera and, in case of long-wave cameras, to specify the glass thickness. This information is used to automatically correct the temperature map on the solar glass, on the basis of the theory of the heat transmission through a body.

III. DIAGNOSTIC METHODOLOGY

After having acquired an IR image, its analysis (consisting on processing, data interpretation, and generation of the final report) requires a lot of skills and experience, but, above all, results extremely time

consuming, because, if a fine diagnostics is desired, many analyses are needed to select and quantify the anomalies. In order to speed up and automatize all of these tasks, we propose the workflow represented in Fig. 2, whose computing steps (violet rectangles) are described in the following subsections.

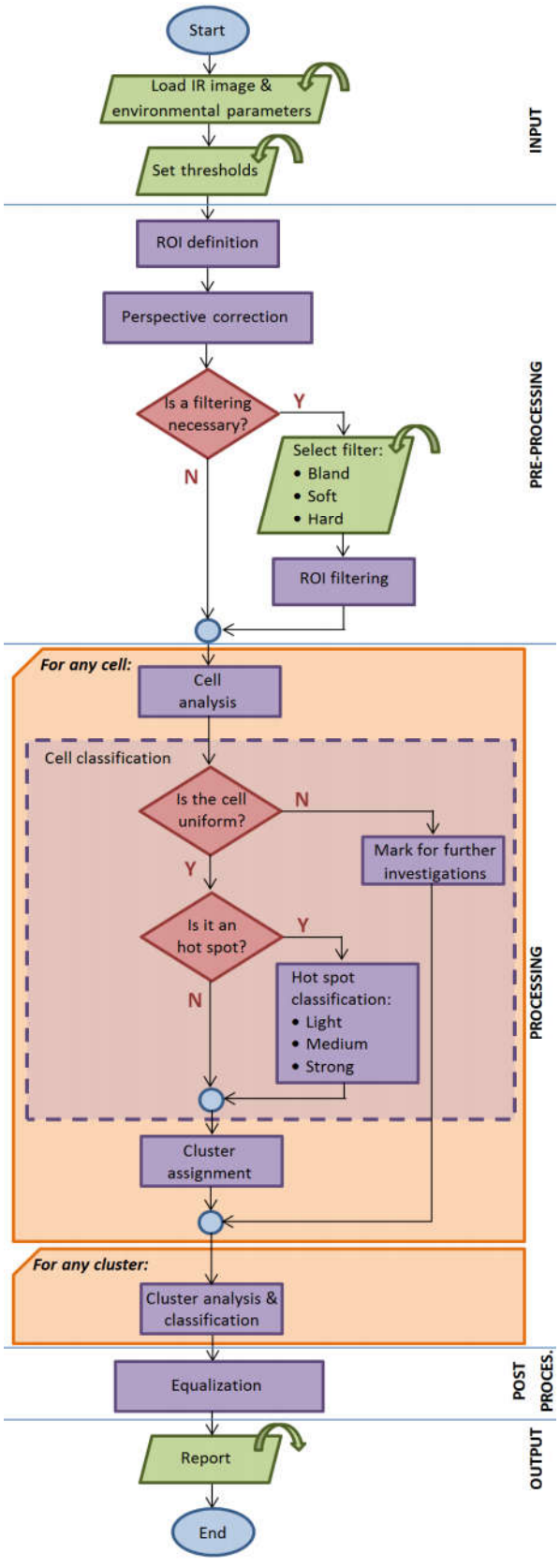

Fig. 2. Proposed diagnostic workflow.

A. *ROI definition*

After the IR image is loaded, and the thresholds are set ("*Load IR image & environmental parameters*" and "*Set thresholds*" INPUT BLOCKS of Fig. 2), the definition of a Region Of Interest (ROI) coincident with the PV module is needed ("*ROI definition*" BLOCK), since an IR image contains almost always objects other than the PV module. This step is two-fold: it allows to deal with smaller images and to focus the attention only on the target of the analysis, i.e. the PV module. For the sake of clarity, Fig. 3 shows a green quadrangle evidencing the ROI, whereas the red markers define the grid subdividing the PV module in cells. This figure (as Figs. 4 e 5 that will be discussed in the following), has been automatically produced by the software platform [21]. As it is clearly visible, the ROI can be obtained extracting the quadrangle individuated by the four vertices of the PV module, and it can be usefully partitioned in as many sub-areas as the total number of PV cells. Each sub-area represents a PV cell, and all the incoming analyses –from now on– will regard only this ROI.

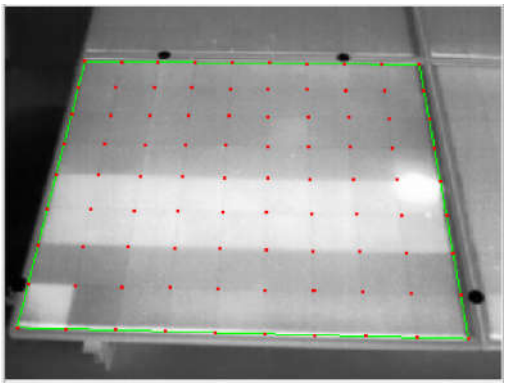

Fig. 3. ROI and grid of PV cells.

B. *Perspective correction*

Because of the perspective introduced by the mutual position of the camera with respect the PV module during the acquisition, the ROI will not be a rectangle, and the areas of the PV cells will be different each other, as it is noticeable by comparing the PV cells in the upper side of the image of Fig. 3, with those in the lower side.

Therefore, the proposed framework applies an affine transformation on the extracted ROI, in order to resize each PV cells to an identical area (as shown in Figs. 4 and 5), and allow to the subsequent analyses to operate on each PV cell in identical conditions.

C. *ROI filtering*

The ROI may be filtered for removing or reducing eventual noise, preparing it to the successive analyses.

The decision about the filter type and how to set its characteristic parameters is not unique, because it depends on the image under consideration, and may be influenced by the environmental conditions and by the acquisition modality. Some suggestions can be found in [22], where it is also proved that the edge detection

can be usefully used, only if applied on a filtered image. With respect to this topic, detailed information about the application of the known Canny's edge detector on PV modules can be found in [11], [14] and [22].

Our experience, built in many diagnostic campaigns on PV plants, shows that the median filter constitutes an effective tool to reduce the noise in IR images of PV modules, since its result (differently from other conventional filters), is not produced by convolutions, but collecting the median values of each pixel-neighborhood. Thanks to this philosophy, almost often the median filter *discards at all* the noisy pixels, instead of taking them in consideration, though weighted by filter coefficients. Nevertheless, in the large casuistry of processed IR images, we have also noticed that a stronger low-pass action than that one allowed by a simple median filter, may be sometimes needed, making necessary other filters. Thus, the workflow provides three possible filtering strategies (bland, soft and hard), each one stronger than the previous one: they may be based either on a median filter, or on a Gaussian filter, or on a cascade of them.

D. Cell analysis

The cell analysis allows investigating the health of each PV cell, through its thermal state. This analysis is performed for each single PV cell, as if this one was not connected to other cells. Its first goal is to separate the uniform cells from the non-uniform ones, where the uniformity is related to the colors (i.e., the temperatures) of the constituting pixels. This task can be performed by calculating, for each PV cell, the variance and the mean of its temperatures. PV cells having variance lower than a pre-defined threshold (see the "*Set thresholds*" INPUT-BLOCK) are considered uniform, otherwise non-uniform.

E. Cell classification

The analysis of non-uniform cells requires particular attention, because sometimes the non-uniformity depends on the internal degradation of the PV cell, whereas other times it is due to external causes, such as dust or dirt on the solar glass. For this reason, the non-uniform cells must be marked for successive specific on site investigations (see the "*N*" branch of the "*Is the cell uniform*" IF-BLOCK).

On the contrary, the uniform PV cells can be immediately studied, by comparing the mean temperatures of the cells with the expected one (that may be determined basing both on the Nominal Operative Cell Temperature -NOCT- and on the environmental conditions, such as irradiance level and air temperature). Nevertheless, since the efficiency of a PV cell decreases as the temperature increases, the only connotation *hot cell* (given to the cells showing over temperature) is not sufficient to determine the severity of the anomalies and the consequent efficiency reduction: therefore, when a rough diagnostics is unsatisfying, to quantify the value of the over temperature is mandatory, in order to get a finer one.

Details on the analysis implementation, both at this level and at the successive *Cluster level* (see paragraph III.G), are given in [20]. Briefly, our approach consists in setting two thresholds, say T_1 and T_2 (see the "*Set thresholds*" INPUT-BLOCK), which classify all the possible cases in three levels of hot cells strictly related to the amount of power losses: light (overtemperature $\leq T_1$), medium (T_1 < overtemperature $\leq T_2$), strong (overtemperature > T_2), as clarified by the example in Fig. 4. Please note that non-uniform cells (masked in black in Fig. 4) may appear (or not) everywhere in each module. Thus, the location of non-uniform cells on the left and right edges of the module in Fig. 4 is absolutely fortuitous, as it is evidenced by other cases of study, discussed in [21].

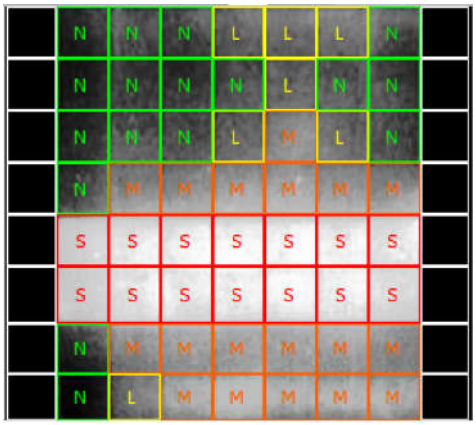

Fig. 4. Non-uniform (masked in black) cells; Normal (green N) cells; Light (yellow L), medium (orange M) and strong (red S) hot cells.

Finally, the hot cells can be classified in function of the main (and more common) defects, taking into account a relation between the over temperature caused by the defect itself and the information reported in Table I, that we have extracted from the Table 2 of the exhaustive study in [23].

TABLE I. DEFECT CLASSIFICATION BY MEANS OF TEMPERATURE DIFFERENCE, EXTRACTED BY TABLE 2 OF [23]

Defect	Over temperature
Bypassed substring	4±2 °C
Cell fracture	2.5÷45 °C or higher
Soldering	12.5±3.6 °C
Shunted cell	1.2±0.4 °C

F. Cluster assignment

Of course, PV cells having similar mean temperatures may occur, and they can be near or far each other. The proposed framework groups these PV cells in families called *clusters* and proposes a second level of analysis, focused on such groups of cells, and not on the single cells.

The clustering is mainly performed basing on the mean temperatures of the PV cells: the "*Cluster*

assignment" BLOCK assigns each PV cell to a cluster characterized by a given temperature range (as it was initialized in the "*Set thresholds*" INPUT-BLOCK), according to the method presented in Part II [20]. Obviously, higher the range, lower the grain and less the number of clusters, and vice versa.

G. Cluster analysis & classification

Once created, the clusters can be analyzed and classified. The valence of this step is twofold, as detailed in the following.

I. To be helpful to the manufacturers, highlighting anomalies: in fact, a PV module may be built by PV cells coming from different productive processes (wafer blocks), thus having different thermal behaviors, even if the datasheet will be unique for the whole module.

II. To allow the end user to monitor at a global level the thermal behavior of the cells: in fact, nowadays the IR analysis is typically performed either yearly or once a semester; thus the *cluster analysis* can highlight whether any cell continues to belong to the same cluster or not, since the composition of a cluster can vary during the life of the PV module and this can be evidenced in periodical reports.

Moreover, cells which were classified as strong hot spot during the "*Cell analysis*" may be characterized by over temperatures of different entities, causing inefficiencies that can significantly vary: for instance, as it has already said in the introduction, an over temperature of 10 °C provokes a 4% inefficiency, while an over temperature of 18 °C causes a 7÷10% decrease. Thus, a more useful information on the state of the PV module can be achieved assigning them to different clusters, so evidencing a finer grain classification than that one achieved for the hot spot.

For example, let us suppose that during the *cell* analysis, 20% of the cells resulted *strong hot cells*, i.e. they showed an over temperature > T_2. If either all of their over temperatures or a large part of them had exceeded T_2 only slightly, of course we would have observed a power loss, but if all of them had outclassed T_2, then we would have seen a much higher power loss than in the previous case. Resuming, depending on the value of the over temperature, the power loss can be more or less significant.

By this way, the "*Cluster analysis & classification*" BLOCK analyzes each cluster basing on the number of enclosed cells, the position inside the PV module, the connectivity among cells (as later explained), and the mean value of the cluster temperature. After that, the BLOCK classifies the clusters sorting them from the *no-problem* ones to the *most critical* one, on the basis of the power loss.

About the previously mentioned connectivity, two cases are possible: a) *jointed cluster*; b) *disjointed cluster*. In the *jointed clusters*, any couple of cells belonging to the cluster can be connected by at least one path which encloses only cells belonging to the cluster itself: therefore, the cluster appears as only one *blob*. Contrarily, in a *disjointed cluster*, at least two cells which cannot be connected by a similar path exist, and the cluster results composed by more than one *blob*. Fig. 5 shows one of the two clusters extracted from the PV module of Fig. 3. This one results a *disjointed cluster* composed by two blobs (respectively containing 16 and 12 PV cells): since the PV module is installed on the roof of a building, and the IR image has been acquired in a sunny day (shaded neither by clouds nor by other objects), the two blobs evidence that those PV cells have internal defects, producing similar over temperature.

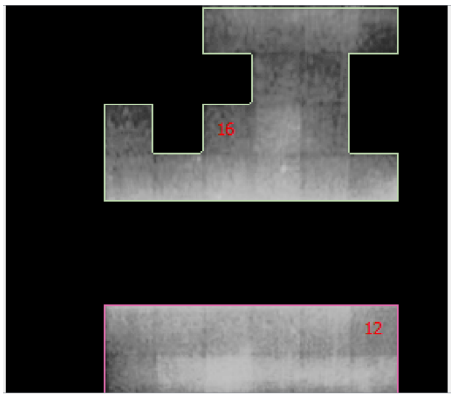

Fig. 5. Cluster of PV cells, constituted by two blobs.

H. Equalization

The last processing block consists on an equalization that does not modify the temperature values, but only their representation in terms of grey-levels. Therefore, it does not act on the diagnostics, being performed just in order to assign the whole available 8-bits dynamic only to the temperature range present on the ROI, i.e., the PV module, with the purpose of providing a better visualization of the results.

IV. Conclusions

This paper proposes a workflow for processing IR images of PV devices, in order to get detailed, quantitative and objective information. Its goal is to perform a twofold diagnosis focused both on the cell level and on the cluster level. In order to make affordable and automatic the entire process, the workflow has been implemented into a software platform, whose description is given in Part II [20].

The analyses resulting from the workflow can help not only the manufacturers to improve their production processes, but also the end users to check and to interpret the real state of health of a single PV module, thus constituting a valid support for the maintenance, because it allows to evaluate the trend of ageing.

For instance, let us consider, as case of study, the defected PV module in Fig. 3, evidently characterized by a bypassed string and a shunted cell (other diagnostic cases are discussed in [20]). The workflow has pointed out several criticalities that were not

perceptible in the source image. Firstly, the two external columns of cells, which, being not uniform, have been masked in black on Fig. 4. Secondly, 7 *light* and 18 *medium* hot spots have been revealed in addition to the expected 14 *strong* hot spots belonging to the bypassed string. Finally, Fig. 5 shows a cluster different from that one related to the bypassed string.

At the best of our knowledge, no current automatic diagnostic approach can give absolute directions *on replacing or not* a certain PV module from a PV plant, since the final decision depends on several factors such as age and ageing trend of the PV module, financial implications, and so on; but the proposed workflow represents a valid support to the technicians for these important evaluations.

REFERENCES

[1] http://www.ise.fraunhofer.de/en/press-and-media/pdfs-zu-presseinfos-englisch/2014/press-release-new-world-record-for-solar-cell-efficiency-at-46-percent.pdf

[2] F. Dimroth, M. Grave, P. Beutel, U. Fiedeler, C. Karcher, T.N.D. Tibbits, E. Oliva, G. Siefer, M. Schachtner, A. Wekkeli, A.W. Bett, R. Krause, M. Piccin, N. Blanc, C. Drazek, E. Guiot, B. Ghyselen, T. Salvetat, A. Tauzin, T. Signamarcheix, A. Dobrich, T. Hannappel, and K. Schwarzburg, "Wafer bonded four-junction GaInP/GaAs//GaInAsP/GaInAs concentrator solar cells with 44.7% efficiency," *Progress in Photovoltaics: Research and Applications*, vol. 22, pp. 277-282, 2014.

[3] http://www.nrel.gov/ncpv/images/efficiency_chart.jpg

[4] E. Skoplaki, and J.A. Palyvos, "On the temperature dependence of photovoltaic module electrical performance: A review of efficiency/power correlations," *Solar Energy*, Vol. 83, pp. 614–624, 2009.

[5] O. Breitenstein, JP Rakotoniaina, M. H. Al Rifai, and M. Werner, "Shunt type in crystalline solar cells," *Progress in photovoltaics research and application*, 12, pp. 529-538, 2004.

[6] J.P. Rakotoniaina, S. Neve, M. Werner, and O. Breitenstein, "Material induced shunts in multicrystalline silicon solar cells," *Proceedings of the Conference on PV in Europe*, Rome, pp. 24-27, 2002.

[7] G. Acciani, O. Falcone, and S. Vergura, "Typical Defects of PV-cells," *Proc. of the IEEE ISIE 2010*, Bari, Italy, pp. 2745-2749, July, 4-7, 2010.

[8] S. Vergura, G. Acciani, and O. Falcone, "Modeling defects of PV-cells by means of FEM," *IEEE-ICCEP2009*, Capri, Italy, pp. 52-56, 2009.

[9] S. Vergura, G. Acciani, and O. Falcone, "3-D PV-cell model by means of FEM," *IEEE-ICCEP 2009*, Capri, Italy, pp 35-40, 2009.

[10] S. Vergura, G. Acciani, and O. Falcone, "A Finite Element Approach to Analyze the Thermal Effect of Defects on Silicon-based PV Cells," *IEEE Trans on Industrial Electronics*, Vol. 59, n. 10, pp. 3860-3867, 2012.

[11] J.A. Tsanakasa, D. Chrysostomoub, P. N. Botsarisa, and A. Gasteratosb, "Fault diagnosis of photovoltaic modules through image processing and Canny edge detection on field thermographic measurements," *International Journal of Sustainable Energy*, doi: 10.1080/14786451.2013.826223 , pp. 1-22, 2013.

[12] Y. Hu, W. Cao, J. Ma, S.J. Finney, and D. Li, "Identifying PV Module Mismatch Faults by a Thermography-Based Temperature Distribution Analysis," *IEEE Transactions on Device and Materials Reliability*, Vol. 14, No. 4, December 2014,

[13] A. Dolara, S. Leva, G. Manzolini, and E. Ogliari, "Investigation on Performance Decay on Photovoltaic Modules: Snail Trails and Cell Microcracks," *IEEE Journal of Photovoltaics*, Vol. 4, n. 5, pp 1204-1211, September 2014.

[14] Y. Hu, W. Cao, J. Wu, B. Ji, and D. Holliday, "Thermography-Based Virtual MPPT Scheme for Improving PV Energy Efficiency Under Partial Shading Conditions," *IEEE Transactions on Power Electronics*, Vol. 29, no. 11, pp. 5667-5672, 2014.

[15] R. Ebner, B. Kubicek, and G. Ujvari, "Non-destructive techniques for quality control of PV modules: Infrared thermography, electro- and photoluminescence imaging," *IEEE-IECON*, pp. 8104-8109, 2013.

[16] S. Johnston, H. Guthrey, F. Yan, K. Zaunbrecher, M. Al-Jassim, P. Rakotoniaina, and M. Kaes, "Correlating Multicrystalline Silicon Defect Types Using Photoluminescence, Defect-band Emission, and Lock-in Thermography Imaging Techniques", *IEEE Journal of Photovoltaics*, Vol. 4, Issue 1, pp. 348-354, 2014.

[17] M. Peloso, L. Meng and C.S. Bhatia, "Combined thermography and luminescence imaging to characterize the spatial performance of multi-crystalline Si wafer solar cells", *IEEE Journal of Photovoltaics*, Vol. 5, Issue 1, pp. 102-111, 2015.

[18] O. Breitenstein, J. Bauer, K. Bothe, D. Hinken, J. Müller, W. Kwapil, M.C. Schubert, W. Warta, "Can luminescence imaging replace lock-in thermography on solar cells?", *IEEE Journal of Photovoltaics*, Vol. 1, Issue 2, pp. 159-167, 2011.

[19] M. Aghaei, F. Grimaccia, C. A. Gonano, S. Leva, "Innovative Automated Control System for PV Fields Inspection and Remote Control", *IEEE Trans. on Industrial Electronics*, Vol. 62, n. 11, pp. 7287-7296, 2015.

[20] www.diss.cloud

[21] S. Vergura, M. Colaprico, M. F. de Ruvo, and F. Marino, "A Quantitative and Computer Aided Thermography-based Diagnostics for PV Devices: Part II – Platform and Results," accepted for publication on *IEEE Journal of Photovoltaics,* DOI (identifier) 10.1109/JPHOTOV.2016.2614860

[22] S. Vergura, and O. Falcone, "Filtering and Processing IR Images of PV Modules," *Renewable Energy & Power Quality Journal*, (ISSN 2172-038X), n.9, 2011.

[23] C. Buerhop, D. Schlegel, M. Niess, C. Vodermayer, R. Weißmann, and C. J. Brabec "Reliability of IR-imaging of PV-plants under operating conditions," *Solar energy materials and solar cells*, vol. 107, pp. 154-164, 2012.